九州大学学術情報リポジトリ
Kyushu University Institutional Repository

Performance Improvement of H-Darrieus Wind Turbine with High Efficiency Vortex Structure Attachment

Anggara, Bayu
Department of Mechanical Engineering, Faculty of Engineering, Universitas Sebelas Maret

Eko Prasetya Budiana
Department of Mechanical Engineering, Faculty of Engineering, Universitas Sebelas Maret

Harsito, Catur
Department of Mechanical Engineering, Vocational School, Universitas Sebelas Maret

Enoki, Koji
Department of Mechanical and Intelligent System Engineering, The University of Electro-Communication

他

https://doi.org/10.5109/6782153

出版情報：Evergreen. 10 (1), pp.496-503, 2023-03. 九州大学グリーンテクノロジー研究教育センター
バージョン：
権利関係：Creative Commons Attribution-NonCommercial 4.0 International

Performance Improvement of H-Darrieus Wind Turbine with High Efficiency Vortex Structure Attachment

Bayu Anggara[1], Eko Prasetya Budiana[1], Catur Harsito[2], Koji Enoki[3], Kim Ki-Seong[4], Indri Yaningsih[1], Dominicus Danardono Dwi Prija Tjahjana[1,*]

[1]Department of Mechanical Engineering, Faculty of Engineering, Universitas Sebelas Maret, Jl. Ir. Sutami 36 A, Surakarta 57126, Indonesia

[2]Department of Mechanical Engineering, Vocational School, Universitas Sebelas Maret, Jl. Ir. Sutami 36 A, Surakarta 57126, Indonesia

[3]Department of Mechanical and Intelligent System Engineering, The University of Electro-Communication, 1-5-1, Chofugaoka, Chofu-shi, Tokyo 182-8585, Japan

[4]School of Mechanical Design Engineering, Faculty of Engineering, Chonnam National University, 50 Daehak-ro, Yeosu, Jeonnam, 550-749, Korea

*Author to whom correspondence should be addressed:
E-mail: ddanardono@staff.uns.ac.id

(Received February 27, 2023; Revised March 24, 2023; accepted March 24, 2023).

Abstract: The H-Darrieus wind turbine could be applied as an alternative electricity generation source. However, their performance is still low, affecting less attention to being used as electricity generation sources. Considering the current condition, the present study provides a numerical simulation of a potential performance enhancement of the H-Darrieus wind turbine by adding a high-efficiency vortex (HEV). HEV owns the ability to control the flow around the blade. HEV causes turbulent flow around the turbine while increasing turbulent kinetic energy. Three different HEV structures in rectangular, trapezoidal, and triangular shapes were attached to the blade to investigate the wind turbine performance. Two-tab angles (β) of 30° and 45° were applied to each structure to investigate the best position of HEV. The blade without HEV was considered as the baseline for the performance evaluation. It is revealed that triangular HEV performed the best with β of 30°, improving the power coefficient by 34% compared to the baseline when the tip speed ratio (TSR) is more than 1.5.

Keywords: H-Darrieus, High Efficiency Vortex, Performance, Wind Turbine

1. Introduction

The demand for electricity consumption per capita increased yearly due to the rapid growth of the world population affecting the increase in total energy consumption. Current energy sources almost entirely come from fossil fuels[1)], which contribute to the high global warming potential. Therefore, the technological development for harvesting renewable energy is now gaining more attention as an alternative energy source to fill the electricity shortage. Wind energy has become one of the renewable energies that are abundantly and widely used as voluntary energy sources by converting using mechanical equipment to generate electrical energy[2)]. The wind turbine is known as the wind energy harvester when enough wind power is available to rotate the blade. The horizontal axis wind turbine (HAWT) type is the most wind turbine construction as they provide the highest performance among others[3,4)] in terms of power. But they are more complex and less practical use. HWAT requires a wider area due to its tower installation, which is most probably around 30 – 100 m in height[5)]. HWAT also generates high noise and requires a more complex structure[6,7)]. On the other hand, the vertical axis wind turbine (VAWT) type has lower performance, but it is more applicable[8,9)]. The VAWT could capture the wind from any direction, which would be useable even in a complex environment.

The current study provides an investigation of VAWT for the H-Darrieus type. Among vertical axis wind turbines (VAWT), the H-Darrieus wind turbine exhibits the highest performance. However, the H-Darrieus wind turbine performs poorly when the incoming airflow is low. The aerodynamic performance of the H-Darrieus wind turbine depends on the flow characteristics around the blade[10)]. High turbulence intensity of wind is preferable

since it gives increased power to the blade. However, strong turbulence intensity might affect the durability and lifetime of the turbine due to the aerodynamic imbalances of the rotor[11]. Not only able to capture the power, but the wind turbine also generates wakes for the downstream[12], which might be undesirable. Therefore, it is mandatory to consider the flow control over the blades when designing the wind turbine. Ashwindran et al.[13] provide a study of how the geometry of the blades affects the flow field when they interact with the wind. They successfully developed mathematical approaches to design a blade morphology where the blade's geometry would affect the drag generated by the turbine.

In the development of wind turbine blade technology, a cross-section of modern blades is now equipped with an airfoil shape that expects to have a maximum lift with low drag[14]. A preferable airfoil must perform a larger lift-over-drag ratio under the wind speed provided. Yossri et al.[15] numerically studied a small-scale wind turbine's airfoil type and size. NACA 4412 type revealed the highest performance with the minimum velocity and maximum vorticity magnitude. At the same time, the turbine's high-stress magnitude increases with the increase in the rotor's size. Mohamed et al.[16] conducted a CFD investigation by comparing 25 types of airfoils and blade pitch angles. It was stated that the LS(1)-0413 airfoil has the highest power coefficient of 0.415, up 10% from NACA 0018. Other parameter designs of airfoil shape affected the performance are chord length[17], height chordwise[18], and leading edge[19]. Under the constraint of the recent study, NACA 0015 airfoil was selected as the blade profile. The airfoil selection was based on the desired pressure distribution at a different angle of attack, which was determined by the wind velocity. In addition, the consideration of the C_L, C_D, and stall characteristics is also included in the selection of the airfoil.

Apart from the airfoil selection, as mentioned above, under the low speed of the wind, the performance of the H-Darrieus still required more effort to improve the performance. Since the performance is greatly influenced by flow over the blade, attaching the vortex generator will be the best option considering their ability to control the flow over the blade. High-efficiency vortex (HEV) is a type of vortex generator which generally applied to enhance heat and mass transfer of internal flow. HEV generates vortices creating shear layers in the front and rear edges of HEV, leading to high shear layers, represented by turbulent kinetic energy[20]; thus, better mixing is achieved. HEV is categorized as a motionless mixer with minimum energy.

Considering the overall merit of HEV current study employs three different structures of HEV (Rectangular, Trapezoidal, and Triangular) into an H-Darrieus wind turbine blade. To the best of our knowledge, the application of HEV on H-Darrieus wind turbine blades is still rarely found. Though existing literature provides an enhancement of the aerodynamic performance of the H-Darrieus wind turbine using vortex generator type, the structure, and attachment of HEV differed. HEV in the current study was installed along the wind turbine blade. The HEV height is determined by the boundary layer thickness of the airfoil[21]. The size is suggested to be 80-100% of the airfoil boundary layer[22]. Not only the structure but the present study also compares the performance of three structures of HEV under two different tab angles (β) of 30° and 45°. The performance will be evaluated by analyzing the power coefficient, torque, and flow characteristics represented by turbulent kinetic energy.

2. Materials and Methods

2.1 Wind Turbine Modeling

A NACA 0015 was chosen as an airfoil blade profile that constructs the h-Darrieus wind turbine. The hub and struts on the turbine were neglected to simplify the simulation. The turbine geometry refers to previous research conducted by Song et al. [23]. The rotor diameter was 1650 mm, and the chord length was 375 mm—turbine installation angle 0°. The blades were attached to the hub or rotor arm at 30% of the chord length. Table 1. Shows turbine parameters used in the current study.

Table 1. H-Darrieus wind turbine Parameter

Parameter	Symbol	Value
Wind (m/s)	V	8
Blade number	N	3
Rotor diameter (mm)	D	1,650
Rotor height (mm)	H	1,000
Blade chord length (mm)	c	375

Figure 1 depicts the 3D model of the H-Darrieus wind turbine blade. It has three blades and rotates counterclockwise.

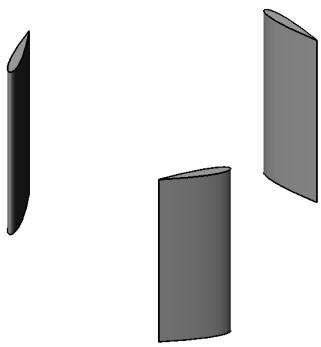

Fig. 1: 3D Model of the H-Darrieus wind turbine blade.

The current study used the CFD formulation to solve the simulation problem. A CFD formulation uses a set of differential equations to define the physical phenomena of fluid flow, momentum, and energy[24].

2.2 High Efficiency Vortex (HEV)

High-Efficiency Vortex (HEV) dimensions were adjusted to the parameters of the turbine blades. Their structure was modified with three shapes; rectangular, trapezoidal, and triangular. The aspect ratio, a ratio of the bottom side (*b*) to the height (*h*) of three structures, was kept constant; while the leading edge (*a*) of HEV was adjusted to give a different shape. Figure 2 illustrates the changes in HEV shapes by decreasing the leading edge dimension from 5.8 to 4.2 for trapezoidal and 0 for triangular.

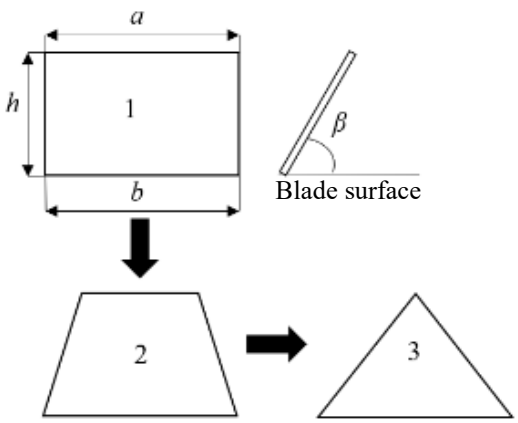

Fig. 2: HEV structures; (1) rectangular, (2) trapezoidal, (3) triangular.

The detail dimension of the HEV is tabulated in Table 2.

Table 2. HEV dimension.

Shape Structure	*a*(mm)	*b*(mm)	*h*(mm)
Rectangular	5.8	5.8	3.2
Trapezoid	4.2	5.8	3.2
Triangular	0	5.8	3.2

The HEV thickness and position towards chord length were constant by 1 mm and 0.25c, respectively. The consideration of selecting the 0.25c position was due to the position being close to the aerodynamics center position, where the pitching moment coefficient does not vary with the angle of attack. For each structure, two different tab angles (*β*) of 30° and 45° were applied to analyze their performance, as shown in Fig. 3. Figure 4 portrays the HEV installed into the blade. The red line shows the HEV positions.

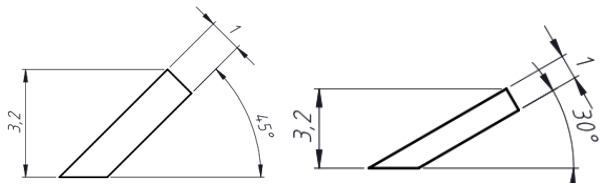

(a) (b)

Fig. 3: Tab angle variation (a) 45° (b) 30°.

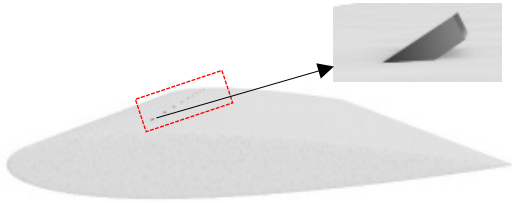

Fig. 4: HEV position on blade.

2.3 CFD modeling preparation and set up

The fluid flow through the wind tunnel is selected for the simulation domain of the H-Darrieus wind turbine simulation. The geometry and dimensions of the simulation domain can be seen in Figure 5. The validation in this simulation refers to Song et al. [23]. This study solves the simulation using ANSYS Fluent software. The simulation method used the Unsteady Reynolds Averaged Navier-Stokes equation (URANS) under transient conditions. The inlet wind speed is 8 m/s with free stream and transient conditions, and the standard temperature and pressure (STP) at 1 atm.

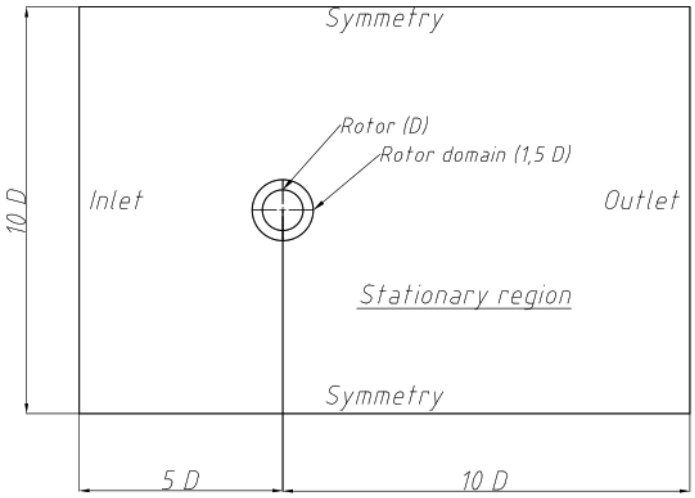

(a)

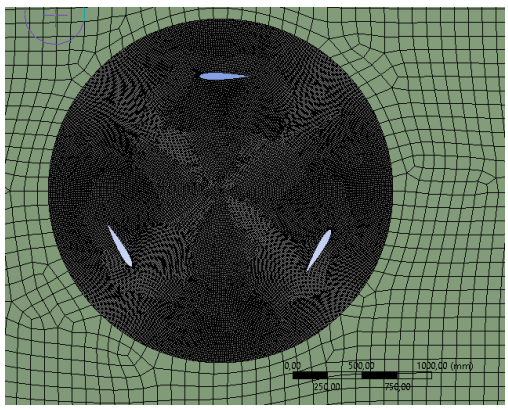

(b)

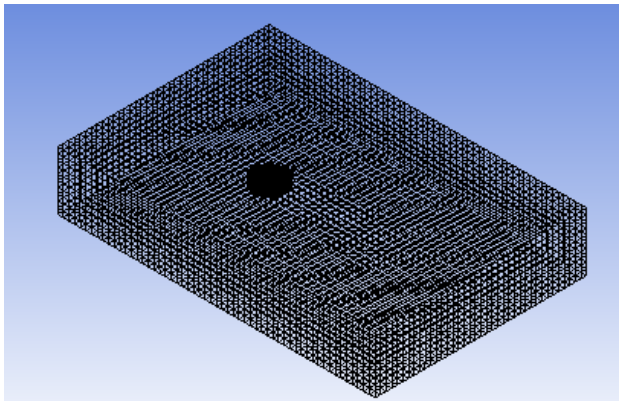

(c)

Fig. 5: (a) 2D view of the domain; (b) 3D view of the meshed domain; (c) Rotor domain mesh.

The computational domain is divided into two parts, namely the inner cylindrical rotating zone and the outer cuboidal stationary zone, as shown in Figure 5. The meshing method in this study is divided into a structure grid for the stationary domain with hexahedron type and an unstructured grid for the rotating domain with tetrahedron type. The body sizing was applied in the rotating zone to improve the accuracy with the element size of 20 mm. In addition, the proximity and curvature function was applied by limiting the local size and proximity size to 1mm. The mesh has been refined around the blade wall.

The mesh fluid zone near the turbine rotates with an angular velocity obtained from the following tip speed ratio Equation (Eq. 1):

$$\gamma = \frac{\omega R}{u} \tag{1}$$

Where γ is the tip speed ratio (TSR), ω is the angular velocity, R is the radius of the turbine and u is the velocity of the wind.

This simulation calculated the time step when the blade takes an angle of 10°. The physical setup time is T/360, where T is the rotation period of the rotor. Equation 2 calculates the time step used in the current study:

$$time\ step = \frac{T}{360\ x\ \Delta\ \theta} \tag{2}$$

The turbulent study in this simulation used a Realizable k-ε viscous model. The second-order spatial and temporal discretization schemes are employed to solve pressure, turbulent kinetic energy, and dissipation rate.

2.4 Model Validation

Validation is carried out by comparing the results of power efficiency (*Cp*) with the existing literature.

The power coefficient, *Cp*, is given by Eq. 3 as follows:

$$Cp = Cm\ x\ TSR \tag{3}$$

where *Cp* is the power coefficient, *Cm* is the moment coefficient, and TSR is the tip speed ratio.

The power coefficient, instantaneous torque coefficients, and average torque coefficient of the turbine at a Tip Speed Ratio (TSR) of 2.0 were compared to the reference study Song et al.[23], as shown in Figure 6. As shown, the discrepancy between the current study and reference[23] falls under acceptable value, ensuring the current simulation's reliability and validity.

Further, the simulation study reported by Song et al.[23] and the experimental study by Castelli[25] have been chosen to validate the modeling methodology. The average *Cm* data for each TSR variation is from 0.5 to 2.5, with a 0.5 increment, comparison can be seen in Figure 7.

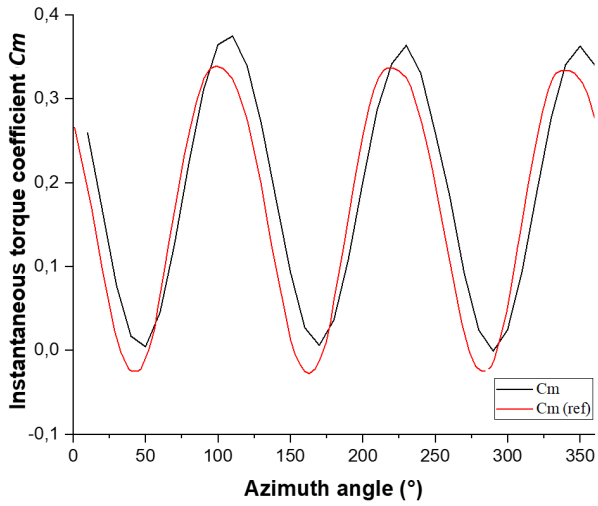

Fig. 6: Comparison of torque coefficient at TSR 2.

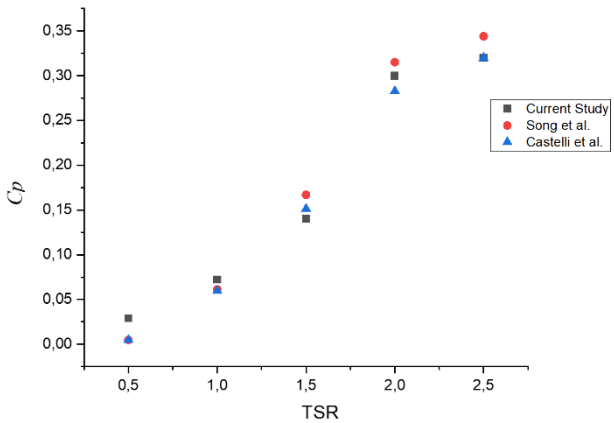

Fig. 7: *Cp* value comparison between current study and references[20,22]

The agreement between this study and previous research is quite good, with a maximum error of 5.04% and an average disparity of 1.05%.

3. Result and discussion

3.1 Moment coefficient

The simulation runs with six different types of HEV variations. The moment coefficient evaluated in this study is taken in the third rotation after the turbine rotates. It is considered that after the third rotation, the turbine torque begins to stabilize. The radar diagram in figure 8 shows a constant change in the value of *Cm* during one rotor rotation.

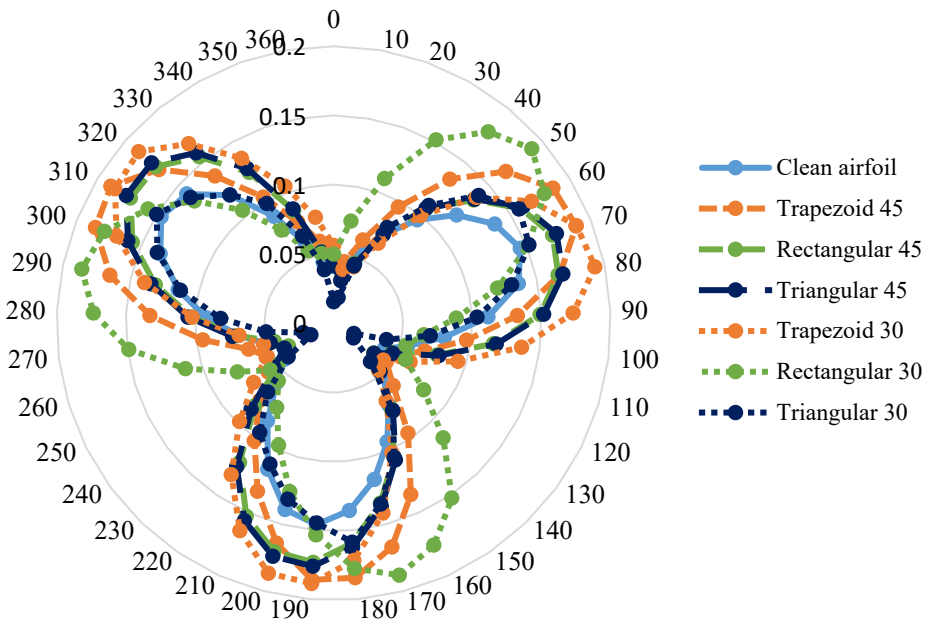

Fig. 8: Moment coefficient (*Cm*) with respect to azimuth angle θ during one rotational period

Figure 8 shows the curve of the turbine torque during rotation for one revolution at TSR = 1.5. The value of the coefficient of moment or torque repeats every 120° since the H-Darrieus wind turbine used three blades. The turbine without HEV has a lower moment coefficient value than the turbine with HEV's addition. The highest instantaneous moment coefficient values are achieved at the azimuth angle θ at positions 70°, 190°, and 310°. Meanwhile, the lowest instantaneous moment coefficient is experienced by the turbine when the azimuth angle θ is at 0°, 130°, and 250°.

3.2 Power coefficient

The power coefficient and TSR graphs are shown in Figure 9. The TSR was analyzed in the range of 0.5 to 2.5.

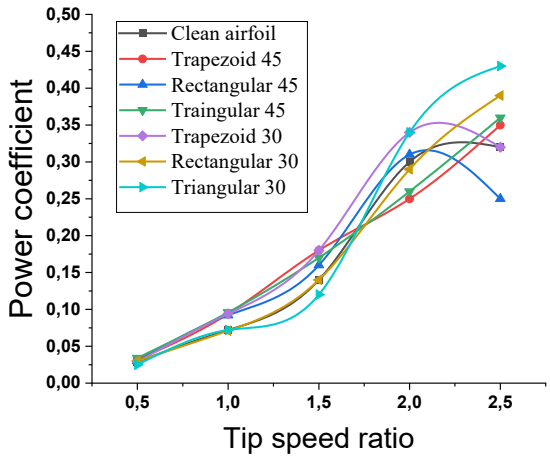

Fig. 9: Power coefficient against tip speed ratio

Figure 9 shows that HEV's presence relatively increases the power coefficient at TSR 1.5, 2.0, and 2.5. At TSR 0.5 and 1.0, there is no significant difference from the addition of this HEV. The *Cp* differences were seen significantly at TSR 1.5, 2.0, and 2.5. The HEV triangular variation obtained the highest *Cp* with a tab angle of 30° at TSR = 2.5 with a *Cp* value of 0.43. The variation of triangular HEV tab angle 30° at low TSR has a relatively low power

coefficient compared to other variations. While the blade without HEV on TSR 2.5 experienced a decreasing trend in power coefficient. It is due to flow separation leading to a dynamic stall. In general, the addition of HEV would delay the occurrence of flow separation, which will enhance at high TSR. It is also revealed that in the trapezoidal HEV shape with a tab angle of 30° and rectangular shape with tab angle of 45°, starting with TSR 2.0, the power coefficient decreases. The use of HEVs will lead to an increase in C_L if the HEVs prevent flow separation at the turbine blade surface. On the other hand, the use of HEVs will also increase the C_D of the turbine blade, which will result in a negative moment that degrades the turbine's performance. The increase in the *Cp* value of the turbine depends on the proportion of the increase in the C_L and C_D values of the turbine due to the addition of HEVs.

From Figure 9, it is also interesting that, in some cases, the HEV addition has a lower performance than the wind turbine with HEV. The performance improvement of the wind turbine depends on the ratio of the lift coefficient enhancement and drag coefficient increment. Therefore, when the power coefficient of the wind turbine with HEV is lower than without HEV, the increased drag coefficient is more prominent than the lift coefficient resulting in a power coefficient reduction.

3.3 Turbulent Kinetic Energy Contour Analysis

Analysis of turbulent kinetic energy in the simulated flow was carried out for all HEV variations at TSR = 1.5. Visualization was carried out at an azimuth angle of 0° and is shown in Figure 10. The HEV attachment to the turbine increased, the turbulent kinetic energy. Flow in the area around the turbine marked with red indicates that turbulent kinetic energy was higher.

The vortex generated by HEV consistently increases the transfer of momentum from the outer area to the boundary layer near the wall[26]. It induces an increase in turbulent kinetic energy in the area close to the wall. Dong and Meng[27] stated there is a relationship between the characteristics of the flow through the micro tab and the resulting turbulent kinetic energy. As can be seen from Fig. 10, as the tab angle increases the turbulent kinetic energy was decreased. When the tab angle increases, the adverse pressure gradient increases due to the suction peak position moving closer to the leading edge of the airfoil blades, and the boundary layer requires more energy to overcome the adverse pressure[28]. In consequence, it is weakens the longitudinal vortex shed behind the VGs.

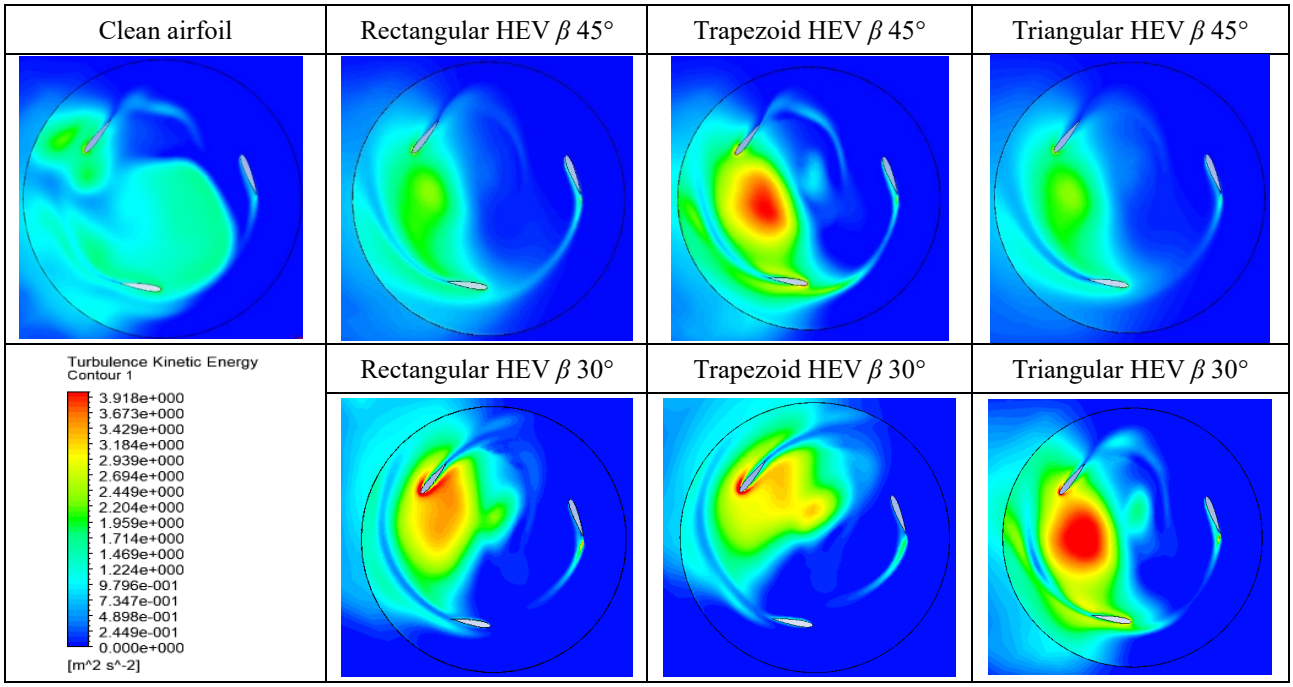

Fig. 10: Visualization of the turbulent kinetic energy of the fluid flow

4. Conclusion

The study of Performance Improvement of the H-Darrieus Wind Turbine with High-Efficiency Vortex Structure Attachment was done using computational fluid dynamics. Results show increased performance by attaching the HEV to the wind turbine blade. HEV effectively enhanced the power coefficient of H-Darrieus wind turbine. VAWT with HEV can delay the occurrence of flow separation in the turbine. The delay of flow separation causes the turbine to achieve a power coefficient of 0.43 at TSR 2.5. It was achieved by the triangular HEV β 30° variation. This value increased by 34% compared to the baseline blade. Additionally, regarding flow characteristics, HEV increases turbulent kinetic energy. In addition, the current results can be used

to support experimental data on subsonic wind tunnels to optimize design validation.

Acknowledgements

This present research work is supported by Universitas Sebelas Maret under the funding scheme Kolaborasi Internasional (KI-UNS) with contract/grant number 228/UN27.22/PT.01.03/2023. The grant is gratefully acknowledged by the authors.

References

1) M.Z. Jacobson, “Review of solutions to global warming, air pollution, and energy security,” *Energy Environ. Sci.*, **2** (*2*) 148–173 (2009). doi:10.1039/b809990c.
2) A.M.M. Ismaiel, and S. Yoshida, "Study on Turbulence Intensity Effect on the Fatigue Lifetime on Wind Tubines," *Evergreen*, **05** (*01*) 25-32 (2018). https://doi.org/10.5109/1929727.
3) W. Xu, G. Li, X. Zheng, Y. Li, S. Li, C. Zhang, and F. Wang, "High-resolution numerical simulation of the performance of vertical axis wind turbines in urban area: Part I, wind turbines on the side of single building," *Renewable Energy*, **177** 461-474 (2021). https://doi.org/10.1016/j.renene.2021.04.071.
4) A. M. Halawa, B. Elhadidi, and S. Yoshida, “Aerodynamic Performance Enhancement Using Active Flow Control on DU96-W-180 Wind Turbine Airfoil,” *Evergreen*, **05** (1) 16–24 (2018). https://doi.org/10.5109/1929723.
5) A. Hosseini, and N. Goudarzi, “Design and cfd study of a hybrid vertical-axis wind turbine by employing a combined bach-type and h-darrieus rotor systems,” *Energy Convers. Manag.*, **189** (*November 2018*) 49–59 (2019). doi:10.1016/j.enconman.2019.03.068.
6) L. Battisti, E. Benini, A. Brighenti, S. Dell’Anna, and M. Raciti Castelli, “Small wind turbine effectiveness in the urban environment,” *Renew. Energy*, **129** 102–113 (2018). doi:10.1016/j.renene.2018.05.062.
7) M.M. Aslam Bhutta, N. Hayat, A.U. Farooq, Z. Ali, S.R. Jamil, and Z. Hussain, “Vertical axis wind turbine - a review of various configurations and design techniques,” *Renew. Sustain. Energy Rev.*, **16** (*4*) 1926–1939 (2012). doi:10.1016/j.rser.2011.12.004.
8) M. Islam, D.S.K. Ting, and A. Fartaj, “Aerodynamic models for darrieus-type straight-bladed vertical axis wind turbines,” Renewable and Sustainable Energy Reviews **12** (4) 1087–1109 (2008). doi:10.1016/j.rser.2006.10.023.
9) T.C. Rudien, D.H. Didane, M.F.M. Batcha, K. Abdullah, S. Mohd, B. Manshoor, and S. Al-Alimi, “Technical feasibility analysis of wind energy potentials in two sites of east malaysia: santubong and kudat,” Evergreen, 8 (2) 271–279 (2021). doi:10.5109/4480703.
10) A.M.M. Ismaiel, S.M. Metwalli, B.M.N. Elhadidi, and S. Yoshida, "Fatigue Analysis of an Optimized HAWT Composite Blade," Evergreen, 04 (02/03) 1-6 (2017). https://doi.org/10.5109/1929656.
11) Z. Xing, M. Chen, J. Cui, Z. Chen, and J. Xu, "Detection of Magnitude and Position of Rotor Aerodynamic Imbalance of Wind Turbines using Convolutional Neural Network," *Renewable Energy*, **197** 1020-1033 (2022). https://doi.org/10.1016/j.renene.2022.07.152.
12) V. Santhanagopalan, M.A. Rotea, and G.V. Iungo, "Performance Optimization of a Wind Turbine Column for Different Incoming Wind Turbulence," *Renewable Energy*, **116** 232-243 (2018). http://dx.doi.org/10.1016/j.renene.2017.05.046.
13) S.N. Ashwindran, A.A. Azizuddin, and A.N. Oumer, "Study of √**2** Conjecture in the Construction of Drag Induced Wind Turbine Blade Morphology," *Evergreen*, 08 (03) 574-585 (2021). https://doi.org/10.5109/4491649.
14) M.M. Takeyeldein, T.M. Lazim, N.A.R. Nik Mohd, I.S. Ishak, and E.A. Ali, "Wind Turbine Design Using Thin Airfoil SD2030," *Evergreen* **06** (02) 114-123 (2019). https://doi.org/10.5109/2321003.
15) W. Yossri, S.B. Ayed, and A. Abdelkefi, "Airfoil type and blade size effects on the aerodynamic performance of small-scale wind turbines: Computational fluid dynamics investigation," *Energy* **229** 120739 (2021). https://doi.org/10.1016/j.energy.2021.120739.
16) M.H. Mohamed, A.M. Ali, and A.A. Hafiz, “CFD analysis for h-rotor darrieus turbine as a low speed wind energy converter,” *Eng. Sci. Technol. an Int. J.*, **18** (*1*) 1–13 (2015). doi:10.1016/j.jestch.2014.08.002.
17) G. Tong, Y. Li, K. Tagawa, and F. Feng, "Effects of blade airfoil chord length and rotor diameter on aerodynamic performance of straight-bladed vertical axis wind turbines by numerical simulation," *Energy* **265** 126325 (2023). https://doi.org/10.1016/j.energy.2022.126325.
18) C. Zhu, Y.i Feng, X. Shen, Z. Dang, J. Chen, Y. Qiu, Y. Feng, and T. Wang, "Effects of the height and chordwise installation of the vane-type vortex generators on the unsteady aerodynamics of a wind turbine airfoil undergoing dynamic stall," *Energy* **266** 126418 (2023). https://doi.org/10.1016/j.energy.2022.126418.
19) Y. Zhang, H. Cao, X. Liu, and L. Qi, "Effect of the leading-edge protuberances on the aeroacoustic and aerodynamic performances of the wind turbine airfoil," *Ocean Engineering* **266** (5) 113153 (2022). https://doi.org/10.1016/j.oceaneng.2022.113153.
20) A. Ghanem, C. Habchi, T. Lemenand, D. Della Valle, and H. Peerhossaini, “Energy Efficiency in Process Industry - High-efficiency vortex (HEV) Multifunctional Heat Exchanger,” *Renew. Energy*, **56**

96–104 (2013). doi:10.1016/j.renene.2012.09.024.
21) U. Fernandez-Gamiz, I. Errasti, R. Gutierrez-Amo, A. Boyano, and O. Barambones, "Computational modelling of rectangular sub-boundary layer vortex generators," *Appl. Sci.*, **8** (*1*) 1–16 (2018). doi:10.3390/app8010138.
22) L. Galera, P. Martinez-Filgueira, U. Fernández-Gámiz, E. Zulueta, J.M. Lopez, and J.M. Blanco, "A triangular vortex generator modeling on a du97-w-300 airfoil by a source term model," *Proc. Inst. Mech. Eng. Part A J. Power Energy*, **233** (*5*) 635–645 (2019). doi:10.1177/0957650919850449.
23) C. Song, G. Wu, W. Zhu, X. Zhang, and J. Zhao, "Numerical investigation on the effects of airfoil leading edge radius on the aerodynamic performance of h-rotor darrieus vertical axis wind turbine," *Energies*, **12** (*19*) (2019). doi:10.3390/en12193794.
24) M. Ahmad, A. Shahzad, F. Akram, F. Ahmad, S. I. A. Shah, "Design optimization of Double-Darrieus hybrid vertical axis wind turbine," Ocean Engineering 254 111171 (2022), https://doi.org/10.1016/j.oceaneng.2022.111171.
25) M. Raciti Castelli, A. Englaro, and E. Benini, "The darrieus wind turbine: proposal for a new performance prediction model based on cfd," *Energy*, **36** (*8*) 4919–4934 (2011). doi:10.1016/j.energy.2011.05.036.
26) D. Kolkman, L.D. de Santana, M.P.J. Sanders, A. V. van Garrel, C.H. Venner, and C. Arc, "Experimental characterization of vortex generators induced noise of wind turbines," *2018 AIAA/CEAS Aeroacoustics Conf.*, (2018). doi:10.2514/6.2018-2800.
27) S. Dong, and H. Meng, "Flow past a trapezoidal tab," *J. Fluid Mech.*, **510** 219–242 (2004). doi:10.1017/S0022112004009486.
28) W.A. Timmer, and R.P.J.O.M. Vanrooy, Wind tunnel results for a 25% thick wind turbine blade airfoil, European Community Wind Energy Conference, Lubeck-Travemunde, Gemany (1993).